Assessing implicit models for nonpolar mean solvation forces: The importance of dispersion and volume terms

Jason A. Wagoner* and Nathan A. Baker†‡

Departments of *Biomedical Engineering and †Biochemistry and Molecular Biophysics, Center for Computational Biology, Washington University, 700 South Euclid Avenue, Campus Box 8036, St. Louis, MO 63110

Edited by Barry H. Honig, Columbia University, New York, NY, and approved April 6, 2006 (received for review January 5, 2006)

Continuum solvation models provide appealing alternatives to explicit solvent methods because of their ability to reproduce solvation effects while alleviating the need for expensive sampling. Our previous work has demonstrated that Poisson-Boltzmann methods are capable of faithfully reproducing polar explicit solvent forces for dilute protein systems; however, the popular solvent-accessible surface area model was shown to be incapable of accurately describing nonpolar solvation forces at atomic-length scales. Therefore, alternate continuum methods are needed to reproduce nonpolar interactions at the atomic scale. In the present work, we address this issue by supplementing the solvent-accessible surface area model with additional volume and dispersion integral terms suggested by scaled particle models and Weeks–Chandler–Andersen theory, respectively. This more complete nonpolar implicit solvent model shows very good agreement with explicit solvent results and suggests that, although often overlooked, the inclusion of appropriate dispersion and volume terms are essential for an accurate implicit solvent description of atomic-scale nonpolar forces.

mean force | solvent-accessible surface area | apolar | hydrophobic

The accurate modeling of solvation is crucial for understanding biomolecular dynamics and energetics. Numerous computational models have been developed for solvation modeling, each offering varying degrees of detail in exchange for computational efficiency. Explicit solvent methods provide atomic resolution of individual solvent molecules; however, the computational cost associated with obtaining converged properties of large systems can quickly become unmanageable. Implicit solvent models, on the other hand, lower the cost of such calculations through an approximate continuum representation of solvation properties.

In general, implicit solvent methods separate solvation energetics into polar and nonpolar contributions. Poisson–Boltzmann (PB) (1–4) and generalized Born (5–10) models are two implicit solvent methods often used to approximate polar solute–solvent interactions by representing the solvent with a simple dielectric continuum model. Solvent-accessible surface area (SASA) models are popular choices for nonpolar solute–solvent interactions; these models assume the nonpolar solvation energy contributions are proportional to surface area (11–17), an argument loosely based on scaled particle theory (SPT) (18, 19). However, the original scaled particle theories (18, 19), and more recent studies by several other groups (20–27), indicate that cavity creation work should depend on both solvent-accessible volume (SAV) and SASA, with a crossover to SASA dominance at large solute sizes. Additionally, it has been suggested that another failing of SASA-based nonpolar solvation models is the lack of appropriate terms to account for attractive van der Waals interactions between solvent and solute atoms (28–39). The above inconsistencies are some possible sources for the wide range of mutually inconsistent SASA "surface tension" parameters (11–13, 40, 41) currently used to model nonpolar interactions. As a solution to this problem, there have been attempts to decompose nonpolar interactions into repulsive and attractive components that can be modeled separately (24, 28–33, 39, 42).

There is particular interest in the ability of implicit solvent models to provide atomic solvation forces with sufficient speed and accuracy for implementation in molecular dynamics simulations (43–45) and other "high-throughput" (15, 16, 46) calculations. However, most models are tested by using only global quantities such as solvation energies (13, 28–33, 41) or simulation rms deviation and stability (33, 44). Although these global metrics provide a "low resolution" assessment of the model quality, they fail to directly test the quantities most relevant to the dynamics simulation: forces. Therefore, as in our previous analyses (47) and similar force-matching multiscale methods used by others (48), we compare mean solvation forces from the explicit solvent simulation with forces from the implicit solvent models.

Previously, we demonstrated that, given appropriate parameters, PB methods are capable of reproducing explicit solvent polar atomic solvation forces with high accuracy for a simple protein system (47). However, we also observed that the popular SASA-based nonpolar force model was unable to accurately reproduce explicit solvent nonpolar solvation forces at atomic resolution. In what follows, we construct a nonpolar solvation force model similar to those just discussed, based on SPT and Weeks–Chandler–Andersen (WCA)-like integral-based methods. The results of this model are then compared with solvation forces obtained from explicit solvent simulations of a dilute protein to assess the accuracy of these very different nonpolar solvation methods.

Theory

As described by Roux and Simonson (49), the potential of mean force (PMF) of a solute in configuration $\mathbf{x}$ can be decomposed into polar $W^{(\mathrm{p})}$ and nonpolar $W^{(\mathrm{np})}$ terms according to the formulae

$$e^{-\beta W^{(\mathrm{np})}(\mathbf{x})} = \frac{\int e^{-\beta[U^{(ss)}(\mathbf{y})+U^{(\mathrm{np})}(\mathbf{x},\mathbf{y})]}d\mathbf{y}}{\int e^{-\beta U^{(ss)}(\mathbf{y})}d\mathbf{y}} \quad [1]$$

$$e^{-\beta W^{(\mathrm{p})}(\mathbf{x})} = \frac{\int e^{-\beta[U^{(ss)}(\mathbf{y})+U^{(\mathrm{np})}(\mathbf{x},\mathbf{y})+U^{(\mathrm{p})}(\mathbf{x},\mathbf{y})]}d\mathbf{y}}{\int e^{-\beta[U^{(ss)}(\mathbf{y})+U^{(\mathrm{np})}(\mathbf{x},\mathbf{y})]}d\mathbf{y}}, \quad [2]$$

where $\beta = (k_{\mathrm{B}}T)^{-1}$ is the inverse thermal energy, $U^{(ss)}$ is the solvent-solvent potential energy, $U^{(\mathrm{np})}$ is the nonpolar portion of the solute–solvent interaction energy, $U^{(\mathrm{p})}$ is the polar portion of the solute–solvent interaction energy, and $\mathbf{y}$ is a high-dimensional coordinate vector for the solvent degrees of freedom. In the present work, we are concerned only with the nonpolar force (Eq. **1**); see

Conflict of interest statement: No conflicts declared.

This paper was submitted directly (Track II) to the PNAS office.

Abbreviations: IFABP, intestinal fatty acid binding protein; MF, mean force; PMF, potential of MF; PB, Poisson-Boltzmann; SASA, solvent-accessible surface area; SAV, solvent-accessible volume; SPT, scaled particle theory; WCA, Weeks–Chandler–Andersen; LJ, Lennard–Jones.

‡To whom correspondence should be addressed. E-mail: baker@biochem.wustl.edu.

Wagoner and Baker (47) for a comparison of polar forces with PB models. The MF on atom i can be obtained by differentiation of the PMF with respect to $\mathbf{x}_i$

$$\mathbf{F}_i^{(\mathrm{np})}(\mathbf{x}) = -\left\langle \frac{\partial U^{(\mathrm{np})}}{\partial \mathbf{x}_i} \right\rangle_{\mathrm{np}}, \qquad [3]$$

where the nonpolar ensemble average of a quantity $q(\mathbf{y})$ is denoted

$$\langle q \rangle_{\mathrm{np}} = \frac{\int q(\mathbf{y}) e^{-\beta[U^{(ss)}(\mathbf{y}) + U^{(\mathrm{np})}(\mathbf{x},\mathbf{y})]} d\mathbf{y}}{\int e^{-\beta[U^{(ss)}(\mathbf{y}) + U^{(\mathrm{np})}(\mathbf{x},\mathbf{y})]} d\mathbf{y}}. \qquad [4]$$

We can rewrite this ensemble average in terms of a density for solvent at position $\mathbf{y}$ given the solute in configuration $\mathbf{x}$:

$$\rho(\mathbf{x}, \mathbf{y}) = \frac{e^{-\beta[U^{(ss)}(\mathbf{y}) + U^{(\mathrm{np})}(\mathbf{x},\mathbf{y})]}}{\int e^{-\beta[U^{(ss)}(\mathbf{y}) + U^{(\mathrm{np})}(\mathbf{x},\mathbf{y})]} d\mathbf{y}} \qquad [5]$$

such that the nonpolar ensemble average of q is $\langle q \rangle_{\mathrm{np}} = \int q(\mathbf{y}) \rho(\mathbf{x}, \mathbf{y}) d\mathbf{y}$. On the basis of WCA perturbation theory (42), Levy and coworkers (32, 33) have argued for a nonpolar solvation PMF of the form $W^{(\mathrm{np})}(\mathbf{x}) = w^{(\mathrm{rep})}(\mathbf{x}) + w^{(\mathrm{att})}(\mathbf{x})$, where $w^{(\mathrm{rep})}$ represents contributions to $W^{(\mathrm{np})}$ from repulsive (usually hard sphere) solute–solvent interactions and $w^{(\mathrm{att})}$ is an integral-based term describing contributions from attractive solute–solvent interactions. Mean solvation forces can be calculated in the usual manner from this PMF decomposition, $\mathbf{F}_i^{(\mathrm{np})}(\mathbf{x}) = \mathbf{f}_i^{(\mathrm{rep})}(\mathbf{x}) + \mathbf{f}_i^{(\mathrm{att})}(\mathbf{x})$, and related to repulsive and attractive components of the potential energy function by $\mathbf{F}_i^{(\mathrm{np})}(\mathbf{x}) = -\langle \partial U^{(\mathrm{rep})}/\partial \mathbf{x}_i \rangle_{\mathrm{np}} - \langle \partial U^{(\mathrm{att})}/\partial \mathbf{x}_i \rangle_{\mathrm{np}}$. The current work uses very similar decompositions based on SPT descriptions for $\mathbf{f}_i^{(\mathrm{rep})}$ and WCA-like integrals for $\mathbf{f}_i^{(\mathrm{att})}$. These models are presented in more detail in the following sections.

Repulsive Nonpolar Solvation Interactions. We approximate the contributions to the PMF and MF from repulsive solute–solvent interactions by assuming a hard-sphere reference system described by a SPT model (18, 19) that includes the volume and area terms:

$$w^{(\mathrm{rep})}(\mathbf{x}) \approx \gamma A(\mathbf{x}) + pV(\mathbf{x}), \qquad [6]$$

where γ is a solvent surface tension parameter, A is a SASA, p is a solvent pressure parameter, and V is a SAV. As mentioned above, the form of this function follows "hard-sphere solvation" theory (50, 51) and is based on the ideas of SPT (18, 19) and other models with similar limiting behavior (20–23). We note that the use of both area and volume terms differs from the more popular area-only treatment of most nonpolar implicit solvent models with some exceptions (see citations above). Models such as Eq. **6** have been generalized for practical use with atom-type-specific γ parameters (12, 14); however, we have observed that use of these per-atom terms does not significantly improve the accuracy of models that include an appropriate $\mathbf{f}_i^{(\mathrm{att})}$ term.

We represent our SPT area A and volume V in terms of the solvent-accessible definition of Lee and Richards (52) and Richmond (53). For this definition, the SAV and SASA are based on a characteristic function $\theta(\mathbf{x}, \mathbf{y}) = \Pi_{i=1}^{N} \theta_i(\mathbf{x}, \mathbf{y})$ defined as a product of per-atom characteristic functions θ_i. These per-atom functions can be written in terms of the Heaviside step function H, e.g., a Boltzmann factor for a hard-sphere solvent–solute potential, $\theta_i(\mathbf{x}, \mathbf{y}) = \Pi_{i=1}^{N} H(\|\mathbf{y} - \mathbf{x}_i\| - \sigma_s - \sigma_i)$, where σ_s is the solvent radius and σ_i is the radius of solute atom i. The characteristic function defines a solvent-inaccessible volume $V(\mathbf{x})$ by $V(\mathbf{x}) = \int_\Omega (1 - \theta(\mathbf{x}, \mathbf{y})) d\mathbf{y}$, where Ω is the problem domain of interest. The surface area $A(\mathbf{x})$ of this volume can be determined by a number of analytic (53, 54) and numerical (55, 56) approaches; we use the Shrake–Rupley numerical approximation (56) implemented in the APBS software package (57).

Forces are usually calculated from SASA/SAV models by differentiation of the free energy with respect to atomic displacements (5, 7, 10), e.g.

$$\mathbf{f}_i^{(\mathrm{rep})}(\mathbf{x}) = \mathbf{f}_i^{(\mathrm{area})}(\mathbf{x}) + \mathbf{f}_i^{(\mathrm{vol})}(\mathbf{x}) = -\gamma \frac{\partial A(\mathbf{x})}{\partial \mathbf{x}_i} - p \frac{\partial V(\mathbf{x})}{\partial \mathbf{x}_i}. \qquad [7]$$

Volume-based force terms have a simple definition:

$$\mathbf{f}_i^{(\mathrm{vol})}(\mathbf{x}) = p \int_\Omega \frac{\partial \theta(\mathbf{x}, \mathbf{y})}{\partial \mathbf{x}_i} d\mathbf{y} = p \int_\Omega \frac{\partial \theta_i(\mathbf{x}, \mathbf{y})}{\partial \mathbf{x}_i} \prod_{j=1, j \neq i}^{N} \theta_j(\mathbf{x}, \mathbf{y}) d\mathbf{y}. \qquad [8]$$

Note that

$$\frac{\partial \theta_i(\mathbf{x}, \mathbf{y})}{\partial \mathbf{x}_i} = -\delta(\|\mathbf{y} - \mathbf{x}_i\| - \sigma_s - \sigma_i) \frac{\mathbf{y} - \mathbf{x}_i}{\|\mathbf{y} - \mathbf{x}_i\|}, \qquad [9]$$

where $\delta(\mathbf{x})$ is the Dirac delta function. This allows us to rewrite the volume derivative as an integral of the unit vector from the atom center over $\Gamma_i(\mathbf{x})$, the solvent-accessible surface of atom i:

$$\begin{aligned} \mathbf{f}^{(\mathrm{vol})}(\mathbf{x}) &= -p \int_{\|\mathbf{y} - \mathbf{x}_i\| = \sigma_s + \sigma_i} \frac{\mathbf{y} - \mathbf{x}_i}{\|\mathbf{y} - \mathbf{x}_i\|} \prod_{j=1, j \neq i}^{N} \theta_j(\mathbf{x}, \mathbf{y}) d\mathbf{y} \\ &= -p \int_{\Gamma_i(\mathbf{x})} \frac{\mathbf{y} - \mathbf{x}_i}{\|\mathbf{y} - \mathbf{x}_i\|} d\mathbf{y}. \end{aligned} \qquad [10]$$

We use the Shrake–Rupley SASA algorithm (56) to determine $\Gamma_i(\mathbf{x})$ for each atom. The SASA derivatives in $\mathbf{f}_i^{(\mathrm{area})}$ can be evaluated in a number of ways, many of them analytic (53–55, 58, 59). However, these expressions tend to be rather complicated and are beyond the scope of the current discussion. We calculate SASA derivatives by a crude numerical finite differencing scheme described in *Computational Methods*.

Attractive Nonpolar Solvation Interactions. We supplement the repulsive contributions to the nonpolar mean solvation forces by the WCA-like (42) attractive integral component:

$$w^{(\mathrm{att})}(\mathbf{x}) = \bar{\rho} \int_\Omega U^{(\mathrm{att})}(\mathbf{x}, \mathbf{y}) g^{(\mathrm{rep})}(\mathbf{x}, \mathbf{y}) d\mathbf{y} \qquad [11]$$

$$\mathbf{f}_i^{(\mathrm{att})}(\mathbf{x}) = -\bar{\rho} \int_\Omega \frac{\partial U^{(\mathrm{att})}(\mathbf{x}, \mathbf{y})}{\partial x_i} g^{(\mathrm{rep})}(\mathbf{x}, \mathbf{y}) d\mathbf{y}, \qquad [12]$$

where $g^{(\mathrm{rep})}$ is the distribution function for the reference repulsive solute–solvent potential. The MF expression follows from Eqs. **3–5**, and the relationship between the density and the distribution functions: $\rho(\mathbf{x}, \mathbf{y}) = \bar{\rho} g^{(\mathrm{rep})}(\mathbf{x}, \mathbf{y})$, where $\bar{\rho}$ is the bulk density. This derivation of the MF is based on Eqs. **3–5**, rather than a simple differentiation of Eq. **11**. As such, our expression for $\mathbf{f}^{(\mathrm{att})}$ does not include a derivative of $g^{(\mathrm{rep})}$. Note that Eq. **11** is based on a perturbative approximation to the true PMF (42), whereas Eq. **12** for $\mathbf{f}^{(\mathrm{att})}$ is an "exact" expression for the MF. Like most perturbative definitions of the force, Eq. **12** is expected to be accurate under conditions away from phase transitions (e.g., de-wetting), which might cause rapid changes in $g^{(\mathrm{rep})}$.

Following models by Gallicchio and coworkers (31–33), we further assume that the reference distribution function can be approximated by our solvent-accessibility characteristic function $g^{(\mathrm{rep})}(\mathbf{x}, \mathbf{y}) \approx \theta(\mathbf{x}, \mathbf{y})$. This potentially severe approximation assumes a uniform solvent distribution outside the solvent-accessible sur-

Table 1. Optimized 6/12 and WCA implicit solvent nonpolar MF parameter values and goodness-of-fit metrics

	MF model 6/12			MF model WCA		
Parameters	Attractive	Repulsive	Total	Attractive	Repulsive	Total
σ_s, Å	0.89 [0.87–0.94]	1.14 [1.04–1.26]	1.55 [1.47–1.8]	0.80 [0.6–0.87]	1.14 [1.05–1.24]	1.13 [1.04–1.20]
γ, cal·mol^{-1}·Å^{-2}	—	20 (1)	5 (1)	—	5 (1)	3 (1)
p, cal·mol^{-1}·Å^{-3}	—	64 (1)	38 (1)	—	35 (1)	36 (1)
r	0.91	0.84	0.89	0.95	0.89	0.90
R	0.95	0.92	0.94	0.95	0.94	0.95
χ^2, 10^{-3} kcal^2·mol^{-2}·Å^{-2}	9.58	31.4	6.99	0.562	4.95	4.50

Separate fits of nonpolar solvation MFs were performed as follows: Attractive, a comparison of attractive implicit (Eq. **12**) and attractive explicit; Repulsive, a comparison of repulsive implicit (Eq. **7**) and repulsive explicit; and Total, a comparison of the total implicit (Eq. **18**) and total explicit nonpolar MFs. Where applicable, standard errors are presented in parentheses; 99% confidence intervals are presented in brackets.

face. Clearly, such an assumption is questionable for a condensed phase system; however, it makes the same uniform density approximation as PB polar solvation models (49) and is necessary to avoid more complicated and expensive integral equation theories (60).

The definitions above assume a decomposition of the solute–solvent interaction potential into attractive integral and repulsive parts: $U^{(\mathrm{np})}(\mathbf{x},\mathbf{y}) = U^{(\mathrm{att})}(\mathbf{x},\mathbf{y}) + U^{(\mathrm{rep})}(\mathbf{x},\mathbf{y})$. In general, it is assumed that the nonpolar solute–solvent potential is pairwise such that the total solute–solvent interaction energy can be decomposed into the interaction of individual atoms with the solvent: $U^{(\mathrm{np})}(\mathbf{x},\mathbf{y}) = \sum_{i=1}^{N} u_i^{(\mathrm{np})}(\mathbf{x}_i,\mathbf{y})$. In particular, we will consider the Lennard–Jones (LJ) solvent–solute interaction potential (61) formulated as

$$u_i^{(\mathrm{np})}(\mathbf{x}_i,\mathbf{y}) = \varepsilon_i\left[\left(\frac{\sigma_i+\sigma_s}{\|\mathbf{x}_i-\mathbf{y}\|}\right)^{12} - 2\left(\frac{\sigma_i+\sigma_s}{\|\mathbf{x}_i-\mathbf{y}\|}\right)^{6}\right],$$

where ε_i measures the depth of the attractive well at $\|\mathbf{x}_i-\mathbf{y}\| = \sigma_i+\sigma_s$ and σ_i, σ_s are the solute atom and solvent radii, respectively, introduced above. The LJ potential can clearly be divided into attractive $u_i^{(\mathrm{att})}$ and repulsive $u_i^{(\mathrm{rep})}$ portions in a number of ways; we will consider two specific decompositions based on the models of Levy and coworkers (32, 33) and the original WCA theory (42). First, we will consider a "6/12" decomposition that splits the individual inverse power potentials (33):

$$u_i^{(\mathrm{att},6/12)}(\mathbf{x}_i,\mathbf{y}) = -2\varepsilon\left(\frac{\sigma_i+\sigma_s}{\|x_i-\mathbf{y}\|}\right)^{6} \qquad [13]$$

$$u_i^{(\mathrm{rep},6/12)}(\mathbf{x}_i,\mathbf{y}) = \varepsilon\left(\frac{\sigma_i+\sigma_s}{\|\mathbf{x}_i-\mathbf{y}\|}\right)^{12}. \qquad [14]$$

We will also examine a "WCA" decomposition of the forces into purely attractive integral and repulsive components (32, 42):

$$u_i^{(\mathrm{att,WCA})}(\mathbf{x}_i,\mathbf{y}) = \begin{cases} -\varepsilon_i & \|\mathbf{x}_i-\mathbf{y}\| < \sigma_i+\sigma_s \\ u_i^{\mathrm{LJ}}(\mathbf{x}_i,\mathbf{y}) & \|\mathbf{x}_i-\mathbf{y}\| \geq \sigma_i+\sigma_s \end{cases} \qquad [15]$$

$$u_i^{(\mathrm{rep,WCA})}(\mathbf{x}_i,\mathbf{y}) = \begin{cases} u_i^{\mathrm{LJ}}(\mathbf{x}_i,\mathbf{y}) + \varepsilon_i & \|\mathbf{x}_i-\mathbf{y}\| < \sigma_i+\sigma_s \\ 0 & \|\mathbf{x}_i-\mathbf{y}\| \geq \sigma_i+\sigma_s \end{cases}. \qquad [16]$$

Regardless of the specific decomposition used above, we will assume that the repulsive portion of the MF [$\mathbf{f}^{(\mathrm{rep})}$] can be modeled by the hard-sphere SPT-like models introduced above (see Eqs. **1** and **7**). Both WCA (42) and inverse power potential (62) repulsive terms have been related to hard-sphere models [although the WCA model generally provides better agreement (42, 60)], making the approximation of $w_i^{(\mathrm{rep})}$ by these SPT-like models plausible.

We propose the following models for nonpolar PMFs

$$W^{(\mathrm{np})}(\mathbf{x}) = \gamma A(\mathbf{x}) + pV(\mathbf{x}) + \bar{\rho}\sum_{i=1}^{N}\int_{\Omega} u_i^{(\mathrm{att})}(\mathbf{x}_i,\mathbf{y})\,\theta(\mathbf{x},\mathbf{y})\,d\mathbf{y} \qquad [17]$$

and MFs

$$\mathbf{F}_i^{(\mathrm{np})}(\mathbf{x}) = -\gamma\frac{\partial A(\mathbf{x})}{\partial \mathbf{x}_i} - p\int_{\Gamma_i(\mathbf{x})}\frac{\mathbf{y}-\mathbf{x}_i}{\|\mathbf{y}-\mathbf{x}_i\|}\,d\mathbf{y} - \bar{\rho}\sum_{i=1}^{N}\int_{\Omega}\frac{\partial u_i^{(\mathrm{att})}(\mathbf{x}_i,\mathbf{y})}{\partial \mathbf{x}_i}\,\theta(\mathbf{x},\mathbf{y})\,d\mathbf{y}. \qquad [18]$$

In what follows, we compare the $\mathbf{F}_i^{(\mathrm{np})}$ values obtained with 6/12 and WCA models for $u^{(\mathrm{att})}$ against explicit solvent simulation results.

Results and Discussion

The following sections compare the implicit solvent models presented above (Eqs. **17** and **18**) to mean solvation forces from explicit solvent simulations. Recall that the implicit solvent models differ in their choice of LJ decomposition: 6/12 with $u_i^{(\mathrm{att})}$ defined by $u_i^{(\mathrm{att},6/12)}$ (see Eq. **13**) and WCA with $u_i^{(\mathrm{att})}$ defined by $u_i^{(\mathrm{att,WCA})}$ (see Eq. **15**).

The implicit solvent nonpolar MF models were parameterized by optimization of the solvent radius σ_s, solvent surface tension γ, and solvent pressure p. Goodness-of-fit for parameter optimization was measured by the mean squared error χ^2 between the implicit and explicit nonpolar MF components. The mean squared error was calculated by using the $3mN$ pairs of force components, where $N = 2{,}114$ is the number of atoms and $m = 8$ is the number of intestinal fatty acid binding protein (IFABP) conformations tested. The solvent radius was optimized by a simple line search, whereas the γ and p parameters were optimized by linear-in-parameters fitting for each σ_s value. Differences between models were assessed by using χ^2 values and a standard F test (63) at the 99% confidence level. The choice of σ_s as an adjustable parameter was motivated by the previous work of Levy *et al.* (32), the desire to preserve LJ parameters from the explicit solvent force fields, and the aesthetic choice of choosing a fixed "bulk" value for solvent density.

The following sections "build up" our model for nonpolar interactions (Eq. **18**) from the popular SASA-only model and thereby demonstrate the importance of the SAV and attractive integral terms. Our standard for all subsequent discussion is the full model (Eq. **18**), which includes both attractive integral (Eq. **12**) and repulsive SPT (Eq. **7**) contributions.

SASA-Only Model. The SASA-only model ($\mathbf{f}_i^{(\mathrm{area})}$ in Eq. **7**) is incapable of accurately reproducing nonpolar solvation forces extracted from explicit solvent simulations. This conclusion is supported by the data in Fig. 1 and in Table 3 and Fig. 2, which are published as supporting information on the PNAS web site and present data comparing SASA-only, SAV-only, and full SPT nonpolar solvation force models with the total explicit solvent nonpolar force. Even with the unrealistic solvent radius of 2.2 Å at the end of our σ_s search interval, the mean squared error $\chi^2 = 19.6\times10^{-3}$ kcal^2·mol^{-2}·Å^{-2}

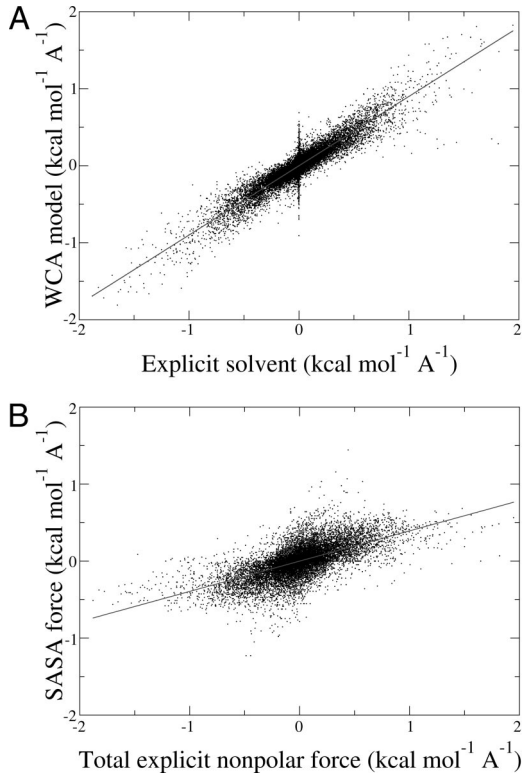

Fig. 1. Comparison of explicit and implicit solvent forces using the optimal parameters in Table 1 for the WCA model (*A*) and the optional parameters in Table 3 for a SASA-only model (*B*).

is much larger than the other models and the Pearson correlation coefficient $R = 0.63$ is very low.

SPT Model. The full SPT model (Eq. **7**) includes both SASA and SAV terms and provides significantly better agreement between implicit and explicit nonpolar solvation forces than SASA-only. Comparison of all goodness-of-fit parameters for the SASA-only model with full SPT model (see Table 3) shows dramatic improvement when both SASA and SAV terms are included. Application of the *F* test indicates that the full SPT model provides a substantial reduction of the mean squared error χ^2 with respect to the SASA-only model with significance well beyond the 99% confidence level. Likewise, visual comparison of implicit–explicit force correlation plots in Fig. 2 *A* and *C* clearly demonstrates the superiority of the full SPT model.

Interestingly, Table 3 shows that SASA coefficient for the full SPT model ($\gamma = 3 \pm 1$ cal·mol^{-1}·Å^{-2}) is much smaller and more poorly constrained than for the SASA-only model ($\gamma = 17.1 \pm 0.7$ cal·mol^{-1}·Å^{-2}) and brings the importance of this term into question. Table 3 also includes data for an SAV-only version of the SPT model; graphical comparison of this SAV-only model and the explicit solvent data are presented in Fig. 3. These data show that the SAV-only model reproduces the explicit solvent nonpolar simulation data with nearly the same fidelity as the full SPT model. Although there is a small, but significant (based on 99% confidence *F* test) reduction in the full SPT model χ^2 compared with the SAV-only model, it is clear that the SAV term provides the largest contribution to the SPT modeling of the nonpolar solvation force. This conclusion is inconsistent with popular SASA-based models of nonpolar solvation forces on the atomic-length scale but agrees with more complete theories of nonpolar solvation (18–27).

Full Model. Although the full SPT model clearly provides a significant improvement over the popular SASA-only model, it does not include the dispersive attractive interactions that have been demonstrated to play an important role in nonpolar solvation energetics (28–38). Given the importance of these attractive contributions, it is not surprising that the full model (Eq. **18**) provides an additional improvement beyond SPT for the representation of nonpolar solvation forces. Both visual (Fig. 1) and quantitative (Tables 1 and 3) comparisons show a substantial improvement in agreement between the implicit and explicit solvent forces when the SPT model is supplemented with an attractive integral term to give Eq. **18**. Application of the *F* test to χ^2 values of the full (6/12 or WCA) and SPT-only models indicates that this improvement is statistically significant to at least a 99% confidence level.

Table 1 also includes comparisons between repulsive and attractive terms in the implicit solvent model with the corresponding MF components from the explicit solvent data. The high correlation (*R*) and regression (*r*) values for these components indicate that the individual components of the implicit solvent model agree well with the explicit solvent data. Interestingly, the 6/12 model produces much higher mean squared errors for the repulsive component than the WCA model; this and other differences between the two implicit models will be discussed in more detail below.

Given the limitations of any implicit solvent model, it is not unexpected that our optimal σ_s solvent radius parameter (1.13 Å for WCA and 1.55 Å for 6/12) is different from the traditional water probe radius of 1.4 Å. Fig. 3, which is published as supporting information on the PNAS web site, illustrates that σ_s (with separately optimized values of γ and p) is relatively loosely constrained by the data and can be changed to 1.4 Å with only a modest increase in χ^2. Therefore, it is possible that σ_s could be fixed at its traditional 1.4-Å value without a substantial increase in the overall modeling error. Alternatively, one could fix σ_s and optimize the solvent density $\bar{\rho}$ or the solvent–solute LJ parameters instead.

Comparison of the 6/12 and WCA Models. It is well known (42, 60) that the WCA decomposition provides a much better model for use with a hard-sphere (or SPT) reference system than a 6/12 decomposition. However, the 6/12-based attractive term is somewhat simpler and has been used in previous studies by Gallicchio and Levy (33) where its use appeared to have little consequence on the accuracy of the predicted energies.

Qualitative differences between the two decomposition schemes are discernible in Fig. 4, which is published as supporting information on the PNAS web site, with overall scatter noticeably smaller for the WCA decomposition. Table 1 presents quantitative differences between the models. The most important difference is the significantly (based on 99% confidence level *F* test) lower mean squared error for WCA compared with 6/12. Table 1 also indicates that WCA does a much better job than 6/12 at reproducing the individual attractive and repulsive force components. Despite these qualitative differences, both models predict very low contributions from SASA to the repulsive free energy. In particular, the surface tensions for these models ($\gamma \approx 3$–5 cal·mol^{-1}·Å^{-2}) are much smaller than popular microscopic surface tension definitions ($\gamma \approx 30$–125 cal·mol^{-1}·Å^{-2}) (11–13, 40, 41) or the "macroscopic" tension of $\gamma \approx$ 75 cal·mol^{-1}·Å^{-2} (13, 20). However, it is worth noting that our γ values are comparable to the 9 cal·mol^{-1}·Å^{-2} obtained by Gallicchio *et al.* (35) for linear alkanes.

Application to Hydrocarbon Solvation Free Energies. At the suggestion of a reviewer, we applied our WCA decomposition methodology to quantify the solvation energies of a series of small hydrocarbon compounds. Unlike large macromolecular complexes, these small hydrocarbons are amenable to solvation free energy calculations (35, 64) and therefore provide a classic framework for testing the validity of the proposed PMF expression (Eq. **17**).

The work of Gallicchio *et al.* (35) provides a detailed decomposition of hydrocarbon solvation free energies into attractive and repulsive contributions. To facilitate direct comparison, we used

Table 2. Comparison of total solvation energies (kcal/mol) for small alkane solutes

Compound	WCA 1.13	WCA 1.04	OPLS	AMBER	Exp.
Methane	2.82	2.10	2.40	2.69	2.00
Ethane	3.53	2.55	2.63	—	1.83
Propane	3.99	2.77	2.89	3.02	1.96
Butane	4.33	2.96	3.21	3.19	2.08
Pentane	5.13	3.50	3.78	—	2.33
Hexane	5.56	3.79	3.78	—	2.49
Isobutane	4.55	3.04	3.03	3.27	2.52
2-Methylbutane	5.04	3.24	3.51	—	2.38
Neopentane	4.97	3.37	3.23	—	2.50
Cyclopentane	3.89	2.40	2.80	—	1.20
Cyclohexane	4.83	2.97	2.34	—	1.23

WCA energy values were obtained by using the methods described with $\sigma_s = 1.13$ and 1.04 Å. OPLS energies were taken from Gallicchio *et al.* (35) by using values in table 2 of their paper. AMBER energies are from Shirts *et al.* (64), ''van der Waals'' values in table II of their paper. Experimental (Exp.) values are from table VII of Cabini *et al.* (65).

their set of hydrocarbon compounds (see Table 2 for the list). All acyclic alkane structures were modeled in the trans conformation; the chair conformer of cyclohexane was used in this study. We applied the WCA form of Eq. **17** to these hydrocarbon structures by using the same procedure as the protein system (see *Computational Methods*). The implicit solvent model was tested for two solvent probe radii; the results are presented in Table 2. Initially, we used the force-optimized WCA parameters of $\sigma_s = 1.13$ Å presented in Table 1. As shown in Table 2, these force-optimized parameters systematically overestimate solvation free energies (OPLS-AA, AMBER, or experimental) for all alkanes. In particular, comparison with the acyclic AMBER test cases gave a Pearson correlation coefficient of $R = 0.93$ but a relative error of $r = 1.46$; comparison with the larger OPLS-AA test set gave a Pearson correlation coefficient of $R = 0.75$ and a relative error of $r = 1.46$. As described (62), nonpolar solute experimental solvation energies were overestimated for all explicit and implicit models tested.

The availability of detailed values for alkane $w^{(rep)}$ and $w^{(att)}$ in the work of Gallicchio *et al.* (35) allowed us to assess the cause of solvation free energy overestimation when using our WCA-based model with $\sigma_s = 1.13$ Å. A detailed comparison of solvation energy components (see Table 4, which is published as supporting information on the PNAS web site) demonstrates that our WCA model with $\sigma_s = 1.13$ Å systematically overestimates both repulsive and attractive components of the solvation free energy. Although it is not optimal to compare the results of our AMBER94-parameterized model with explicit solvent results from the OPLS-AA force field, such comparison is sufficient to demonstrate the sources of overestimation with $\sigma_s = 1.13$ Å. Furthermore, comparison of OPLS and AMBER94 solvation energies calculations by Shirts *et al.* (64) revealed very similar energies for small nonpolar side-chain analogues. The overestimation of both energy components suggests reduction of the probe radius σ_s to decrease the repulsive (by decreasing SAV and SASA) and attractive (by integrating over more favorable regions of the potential) portions of the solvation free energy. Recall that our optimal choice of $\sigma_s = 1.13$ was taken from a 99% confidence interval of $1.04 \leq \sigma_s \leq 1.20$ (compare Table 1 and Fig. 3). To examine the effect of σ_s on agreement with explicit solvent results, we recalculated solvation energies by using our WCA model, $\sigma_s = 1.04$ Å, and the corresponding optimal $\gamma = 3$ cal·mol^{-1}·Å^{-2} and $P = 35$ cal·mol^{-1}·Å^{-3}. Energy results for $\sigma_s = 1.04$ Å are presented in Table 2; free energy components are presented in Table 4. Comparison of the $\sigma_s = 1.04$-Å results in Table 2 with the other explicit solvent energies now gives a Pearson correlation coefficient of $R = 0.91$ and a relative error of $r = 1.01$ for AMBER and a Pearson correlation coefficient of $R = 0.83$ and a relative error of $r = 0.98$ for OPLS-AA. When only acyclic alkanes are considered in the OPLS-AA comparison, the Pearson correlation coefficient is $R = 0.96$ and the relative error is $r = 0.97$. In short, there is a choice of σ_s within the 99% confidence interval of the force-optimized value, which reproduces both AMBER and OPLS alkane solvation energies with good accuracy.

The detailed comparison of solvation energy components in Table 4 provides additional support for our proposed use of both SAV and SASA terms in the repulsive (or cavity) component of the free energy. In particular, the SAV/SASA model for $w^{(rep)}$ (Eq. **6**) correlates very strongly (Pearson $R > 0.99$ for $\sigma_s = 1.13$ or 1.04 Å) with the OPLS-AA repulsive explicit solvent contributions from the work of Gallicchio *et al.* (35). This agreement indicates that whereas a SASA-dominated nonpolar model may be sufficient to reproduce repulsive contributions to solvation free energies it is not necessary. This result is somewhat surprising, because many models predict a ''crossover'' to SASA-dominated cavity formation energies at macroscopic length scales (20–27). However, given the relatively small size of the alkanes tested here, it is possible that we have not yet reached the length scales where such a crossover might occur.

Conclusions

We have demonstrated that the popular SASA model cannot reproduce nonpolar solvation forces from explicit solvent simulations; however, an implicit solvent model including both WCA-like attractive integral and full SPT (with both SAV and SASA components) repulsive terms gives very good agreement. Additionally, we have shown that parameters of the WCA-like implicit model optimized against solvation MFs are also capable of reproducing solvation energies for small alkane compounds. Contrary to many popular nonpolar solvation models, the SASA derivative contributes very little to our WCA-like treatment; the most important elements are derivatives of the SAV and attractive integral terms. The nonpolar solvation force model presented in this article offers a substantial improvement over the popular SASA-only and is sufficiently simple to permit routine use in implicit solvent simulations without a substantial increase in computational overhead.

The failure of SASA models to accurately predict solvation forces raises serious questions about the validity of their widespread application in the interpretation of nonpolar contributions to protein folding, protein–protein binding, and protein–nucleic acid interactions. In particular, the inaccuracy of SASA-only nonpolar solvation forces suggests that these models cannot correctly discriminate between different conformational states and therefore could produce systemic bias when used in simulations or in the interpretation of experimental thermodynamic data. This suggestion is supported by the alanine dipeptide simulations of Su and Gallicchio (39), which indicates that implicit solvent simulations with SASA-only models produce qualitatively inaccurate PMFs. Further evidence is provided by the work of Drozdov *et al.* (66), which demonstrates that peptide–solvent interaction energies for a variety of alanine dipeptide show weak anticorrelation with SASA. The accurate treatment of nonpolar energies and forces is vital for understanding any biomolecular process that involves substantial changes in solvent accessibility, e.g., binding free energies, folding and stability, or even equilibrium fluctuations of biomolecules with highly flexible loops. The inability of SASA-only models to provide such accuracy indicates a need to move to a more complete nonpolar theory in both simulations and the interpretation of experimental data.

Computational Methods

Protein Conformational Sampling. Implicit and explicit solvation forces and energies were compared (see below) for a set of eight conformations of the IFABP. These conformations were obtained, as described (47), from conformational clustering of 2.5-ns molecular dynamics simulation starting from an IFABP NMR model (Protein Data Bank ID code 1AEL) (67) in the presence of ≈160 mM NaCl (25 Na^+ and 26 Cl^- ions). The simulation was performed

at 300 K and 1 atm pressure by using AMBER 7 software (68) with the AMBER94 force field (69).

Explicit Solvent Sampling. We obtained mean nonpolar solvation quantities of the form in Eq. **4** from explicit solvent simulations of IFABP as described (47). TIP3P (transferable intermolecular potential 3 point) (70) solvent configurations were sampled around each of the eight static conformations of IFABP (described above). Solvent sampling was performed for each of the IFABP conformations with the IFABP structure constrained by the belly dynamics algorithm (68). To simulate the nonpolar ensemble, electrostatic solute-solvent interactions are turned off by setting the protein charges to zero. Snapshots were taken every 4 ps, resulting in 250 conformations for each trajectory used in the analyses. Mean solvation forces were calculated by averaging over these conformations. The exact average of a quantity q in Eq. **6** was approximated by $\langle q \rangle_{\rm np} \approx \frac{1}{M} \Sigma_{j=1}^{N} q(\mathbf{x}(t_j))$ for M solvent configuration snapshots $\mathbf{x}(t_j)$ from the nonpolar ensemble simulations. The repulsive and attractive explicit solvent LJ forces were calculated by averaging the derivatives of $u_{\rm i}^{\rm (rep)}$ and $u_{\rm i}^{\rm (att)}$ as defined above for each atom.

Implicit Solvent Model Implementation. All of the implicit nonpolar solvation models described above have been implemented in a developmental version of the APBS electrostatics package (57), which is available from http://apbs.sf.net. For the integral-based methods, we used solvent number densities appropriate for bulk water at 1 g·cm^{-3} density, $\bar{\rho} = 0.033428$ Å^{-3}.

The terms of $\mathbf{F}_i^{\rm (np)}$ were calculated based on Eq. **18**. The Shrake–Rupley method (56) was used to construct solvent-accessible surfaces (e.g., for use in calculating A and Γ_i) discretized with 2,000 surface quadrature points by using AMBER94 van der Waals radii for σ_i (69). As described above, the value of σ_s (solvent probe radius) for these surface was treated as a parameter used in fitting implicit solvent model parameters to explicit solvent results. We calculated surface area derivatives via finite differencing through 0.05-Å displacements of the atomic positions.

The integral term (Eq. **12**) of $\mathbf{F}_{\rm i}^{\rm (np)}$ was calculated over a 14-Å spherical subdomain surrounding atom i discretized into a Cartesian grid of 1.0 Å or finer spacing. Quadratures were calculated over this grid by using Simpson's rule. Contributions from outside of the 14-Å sphere were negligible. The integration results were relatively insensitive to quadrature grid spacings finer than 2.5-Å resolution for solvent probe radii as small as 0.8 Å.

Representative timing information for the SASA, SAV, and integral calculations is provided in *Supporting Text*, which is published as supporting information on the PNAS web site.

We thank Rohit Pappu for helpful discussions on this topic, N.A.B. group members for their reading of the document, and anonymous reviewers for their suggestions. This research was supported, in part, by an Alfred P. Sloan Research Fellowship (to N.A.B.) and National Institutes of Health Grant R01 GM069702.

1. Honig, B. & Nicholls, A. (1995) *Science* **268,** 1144–1149.
2. Davis, M. E. & McCammon, J. A. (1990) *Chem. Rev.* **94,** 7684–7692.
3. Baker, N. A. (2005) *Curr. Opin. Struct. Biol.* **15,** 137–143.
4. Lamm, G. (2003) in *Reviews in Computational Chemistry*, eds. Lipkowitz, K. B., Larter, R. & Cundari, T. R. (Wiley, Hoboken, NJ), Vol. 19, pp. 147–366.
5. Feig, M. & Brooks, C. L., III (2004) *Curr. Opin. Struct. Biol.* **14,** 217–224.
6. Schaefer, M. & Karplus, M. (1996) *J. Phys. Chem.* **100,** 1578–1599.
7. Onufriev, A., Case, D. A. & Bashford, D. (2002) *J. Comput. Chem.* **23,** 1297–1304.
8. Zhu, J., Alexov, E. & Honig, B. (2005) *J. Phys. Chem. B* **109,** 3008–3022.
9. Still, W. C., Tempczyk, A., Hawley, R. C. & Hendrickson, T. (1990) *J. Am. Chem. Soc.* **112,** 6127–6129.
10. Bashford, D. & Case, D. A. (2000) *Annu. Rev. Phys. Chem.* **51,** 129–152.
11. Chothia, C. (1974) *Nature* **248,** 338–339.
12. Eisenberg, D. & McLachlan, A. D. (1986) *Nature* **319,** 199–203.
13. Sharp, K. A., Nicholls, A., Fine, R. F. & Honig, B. (1991) *Science* **252,** 106–109.
14. Wesson, L. & Eisenberg, D. (1992) *Protein Sci.* **1,** 227–235.
15. Massova, I. & Kollman, P. A. (2000) *Perspect. Drug Discov. Des.* **18,** 113–135.
16. Swanson, J. M. J., Henchman, R. H. & McCammon, J. A. (2004) *Biophys. J.* **86,** 67–74.
17. Spolar, R. S., Ha, J. H. & Record, M. T. J. (1989) *Proc. Natl. Acad. Sci. USA* **86,** 8382–8385.
18. Pierotti, R. A. (1976) *Chem. Rev.* **76,** 717–726.
19. Stillinger, F. (1973) *J. Solution Chem.* **2,** 141–158.
20. Lum, K., Chandler, D. & Weeks, J. D. (1999) *J. Phys. Chem. B* **103,** 4570–4577.
21. Huang, D. M & Chandler, D. (2000) *Proc. Natl. Acad. Sci. USA* **97,** 8324–8327.
22. Hummer, G., Garde, S., Garcia, A. E. & Pratt, L. R. (2000) *Chem. Phys.* **258,** 349–370.
23. Rajamani, S., Truskett, T. M. & Garde, S. (2005) *Proc. Natl. Acad. Sci. USA* **102,** 9475–9480.
24. Manjari, S. R. & Kim, H. J. (2005) *J. Chem. Phys.* **123,** 014504.
25. Kang, Y. K., Nemethy, G. & Scheraga, H. A. (1987) *J. Phys. Chem.* **91,** 4105–4109.
26. Gibson, K. D. & Scheraga, H. A. (1967) *Proc. Natl. Acad. Sci. USA* **58,** 420–427.
27. Dzubiella, J., Swanson, J. M. J. & McCammon, J. A. (2006) *J. Chem. Phys.* **124,** 084905.
28. Zacharias, M. (2003) *J. Phys. Chem. A* **107,** 3000–3004.
29. Floris, F. & Tomasi, J. (1989) *J. Comput. Chem.* **10,** 616–627.
30. Floris, F. M., Tomasi, J. & Ahuir, J. L. P. (1991) *J. Comput. Chem.* **12,** 784–791.
31. Gallicchio, E., Zhang, L. Y. & Levy, R. M. (2002) *J. Comput. Chem.* **23,** 517–529.
32. Levy, R. M., Zhang, L. Y., Gallicchio, E. & Felts, A. K. (2003) *J. Am. Chem. Soc.* **125,** 9523–9530.
33. Gallicchio, E. & Levy, R. M. (2004) *J. Comput. Chem.* **25,** 479–499.
34. Pitera, J. W. & van Gunsteren, W. F. (2001) *J. Am. Chem. Soc.* **123,** 3163–3164.
35. Gallicchio, E., Kubo, M. M. & Levy, R. M. (2000) *J. Phys. Chem. B* **104,** 6271–6285.
36. Choudhury, N. & Pettitt, B. M. (2005) *J. Am. Chem. Soc.* **127,** 3556–3567.
37. Choudhury, N. & Pettitt, B. M. (2005) *Mol. Simul.* **31,** 457–463.
38. Malham, R., Johnstone, S., Bingham, R. J., Barratt, E., Phillips, S. E. V., Laughton, C. A. & Homans, S. W. (2005) *J. Am. Chem. Soc.* **127,** 17061–17067.
39. Su, Y. & Gallicchio, E. (2004) *Biophys. Chem.* **109,** 251–260.
40. Elcock, A. H., Sept, D. & McCammon, J. A. (2001) *J. Phys. Chem. B* **105,** 1504–1518.
41. Sitkoff, D., Sharp, K. A. & Honig, B. (1994) *Biophys. Chem.* **51,** 397–403; discussion 404–409.
42. Weeks, J. D., Chandler, D. & Andersen, H. C. (1971) *J. Chem. Phys.* **54,** 5237–5247.
43. Luo, R., David, L. & Gilson, M. K. (2002) *J. Comput. Chem.* **23,** 1244–1253.
44. Lu, Q. & Luo, R. (2003) *J. Chem. Phys.* **119,** 11035–11047.
45. Smart, J. L., Marrone, T. J. & McCammon, J. A. (1997) *J. Comput. Chem.* **18,** 1750–1759.
46. Hsieh, M.-J. & Luo, R. (2004) *Proteins* **56,** 475–486.
47. Wagoner, J. & Baker, N. A. (2004) *J. Comput. Chem.* **25,** 1623–1629.
48. Izvekov, S., Parrinello, M., Bumham, C. J. & Voth, G. A. (2004) *J. Chem. Phys.* **120,** 10896–10913.
49. Roux, B. & Simonson, T. (1999) *Biophys. Chem.* **78,** 1–20.
50. Reiss, H., Frisch, H. L. & Lebowitz, J. L. (1959) *J. Chem. Phys.* **31,** 369–380.
51. Rosenfeld, Y. (1988) *J. Chem. Phys.* **89,** 4272–4287.
52. Lee, B. & Richards, F. M. (1971) *J. Mol. Biol.* **55,** 379–400.
53. Richmond, T. J. (1984) *J. Mol. Biol.* **178,** 63–89.
54. Edelsbrunner, H. & Koehl, P. (2003) *Proc. Natl. Acad. Sci. USA* **100,** 2203–2208.
55. Richards, F. M. (1985) *Methods Enzymol.* **115,** 440–464.
56. Shrake, A. & Rupley, J. A. (1973) *J. Mol. Biol.* **79,** 351–364.
57. Baker, N. A., Sept, D., Joseph, S., Holst, M. J. & McCammon, J. A. (2001) *Proc. Natl. Acad. Sci. USA* **98,** 10037–10041.
58. Sridharan, S., Nicholls, A. & Sharp, K. A. (1994) *J. Comput. Chem.* **16,** 1038–1044.
59. Connolly, M. L. (1985) *J. Am. Chem. Soc.* **107,** 1118–1124.
60. Hansen, J.-P. & McDonald, I. R. (2000) *Theory of Simple Liquids* (Academic, San Diego), 2nd Ed.
61. Allen, M. P. & Tildesley, D. J. (1987) *Computer Simulation of Liquids* (Clarendon, Oxford).
62. Heyes, D. M. & Powles, J. G. (1998) *Mol. Phys.* **95,** 259–267.
63. Press, W. H., Teukolsky, S. A., Vetterling, W. T. & Flannery, B. P. (1992) *Numerical Recipes in C* (Cambridge Univ. Press, New York).
64. Shirts, M. R., Pitera, J. W., Swope, W. C. & Pande, V. S. (2003) *J. Chem. Phys.* **119,** 5740–5761.
65. Cabani, S., Gianni, P., Mollica, V. & Lepori, L. (1981) *J. Solution Chem.* **10,** 563–595.
66. Drozdov, A. N., Grossfield, A. & Pappu, R. V. (2004) *J. Am. Chem. Soc.* **126,** 2574–2581.
67. Hodson, M. E. & Cistola, D. P. (1997) *Biochemistry* **36,** 2278–2290.
68. Pearlmann, D. A., Case, D. A., Caldwell, J. W., Ross, W. S., Cheatham, T. E., III, DeBolt, S., Ferguson, D., Seibel, G. & Kollman, P. (1995) *Comput. Phys. Commun.* **91,** 1–41.
69. Cornell, W. D., Cieplak, P., Bayly, C. I., Gould, I. R., Merz, K. M., Ferguson, D. M., Spellmeyer, D. C., Fox, T, Caldwell, J. W. & Kollman, P. A. (1995) *J. Am. Chem. Soc.* **117,** 5179–5197.
70. Jorgensen, W. L., Chandrasekhar, J. & Madura, J. D. (1983) *J. Chem. Phys.* **79,** 926–935.

Corrections

CHEMISTRY, BIOPHYSICS. For the article "Assessing implicit models for nonpolar mean solvation forces: The importance of dispersion and volume terms," by Jason A. Wagoner and Nathan A. Baker, which appeared in issue 22, May 30, 2006, of *Proc Natl Acad Sci USA* (103:8331–8336; first published May 18, 2006; 10.1073/pnas.0600118103), the authors note that an error in the implementation of Eq. **10** in the original paper led to improper scaling of the solvent-accessible volume forces for highly exposed surface atoms. The error in the original implementation of Eq. **10** affects Tables 1 and 2 of the original manuscript as well as Tables 3 and 4 and Figs. 2 *B* and *C* and 3 in the original supporting information. Corrected versions of Tables 1 and 2 appear below. A correction to the supporting information has been published online. This error does not affect the conclusions of the article.

Table 1. Optimized 6/12 and WCA implicit solvent nonpolar MF parameter values and goodness-of-fit metrics

	MF model 6/12			MF model WCA		
Parameters	Attractive	Repulsive	Total	Attractive	Repulsive	Total
σ_s, Å	0.89 [0.87–0.91]	1.29 [1.16–1.44]	1.68 [1.57–1.80]	0.8 [0.73–0.86]	1.29 [1.18–1.41]	1.25 [1.16–1.39]
γ, cal·mol^{-1}·Å^{-2}	—	15(1)	1(1)	—	2(1)	0(1)
p, cal·mol^{-1}·Å^{-3}	—	94(2)	55(2)	—	52(2)	55(2)
r	0.88	0.56	0.83	0.84	0.87	0.86
R	0.97	0.91	0.94	0.97	0.94	0.94
χ^2, 10^{-3} kcal^2·mol^{-2}·Å^{-2}	6.99	3.35	6.47	0.56	4.87	4.63

Separate fits of nonpolar solvation MFs were performed as follows: Attractive, a comparison of attractive implicit (Eq. **15**) and attractive explicit; Repulsive, a comparison of repulsive implicit (Eq. **10**) and repulsive explicit; and Total, a comparison of the total implicit (Eq. **21**) and total explicit (Eq. **8**) nonpolar MFs. Where applicable, standard errors are presented in parentheses; 99% confidence intervals (see text) are presented in brackets.

Table 2. Comparison of total solvation energies (kcal/mol) for small alkane solutes

Compound	WCA 1.25	WCA 0.65	OPLS	AMBER	Exp.
Methane	6.40	1.93	2.40	2.69	2.00
Ethane	8.41	2.25	2.63	—	1.83
Propane	10.5	2.84	2.89	3.02	1.96
Butane	11.8	2.93	3.21	3.19	2.08
Pentane	13.7	3.48	3.78	—	2.33
Hexane	15.6	3.90	3.78	—	2.49
Isobutane	12.0	3.16	3.03	3.27	2.52
2-Methylbutane	13.4	3.45	3.51	—	2.38
Neopentane	13.2	3.46	3.23	—	2.50
Cyclopentane	11.3	2.25	2.80	—	1.20
Cyclohexane	13.7	3.18	2.34	—	1.23

WCA energy values were obtained by using the methods described in the text with $\sigma_s = 1.25$ and 0.65 Å. OPLS energies were taken from Gallicchio *et al.* (35) by using values in table 2 of their paper. AMBER energies are from Shirts *et al.* (64), 'van der Waals' values in table II of their paper. Experimental (Exp.) values are from table VII of Cabini *et al.* (65).

www.pnas.org/cgi/doi/10.1073/pnas.0610582103

NEUROSCIENCE. For the article "Loss of AP-3 function affects spontaneous and evoked release at hippocampal mossy fiber synapses," by Anita Scheuber, Rachel Rudge, Lydia Danglot, Graca Raposo, Thomas Binz, Jean-Christophe Poncer, and Thierry Galli, which appeared in issue 44, October 31, 2006, of *Proc Natl Acad Sci USA* (103:16562–16567; first published October 20, 2006; 10.1073/pnas.0603511103), the authors note that Fig. 3*g* was labeled incorrectly. The corrected figure and its legend appear below.

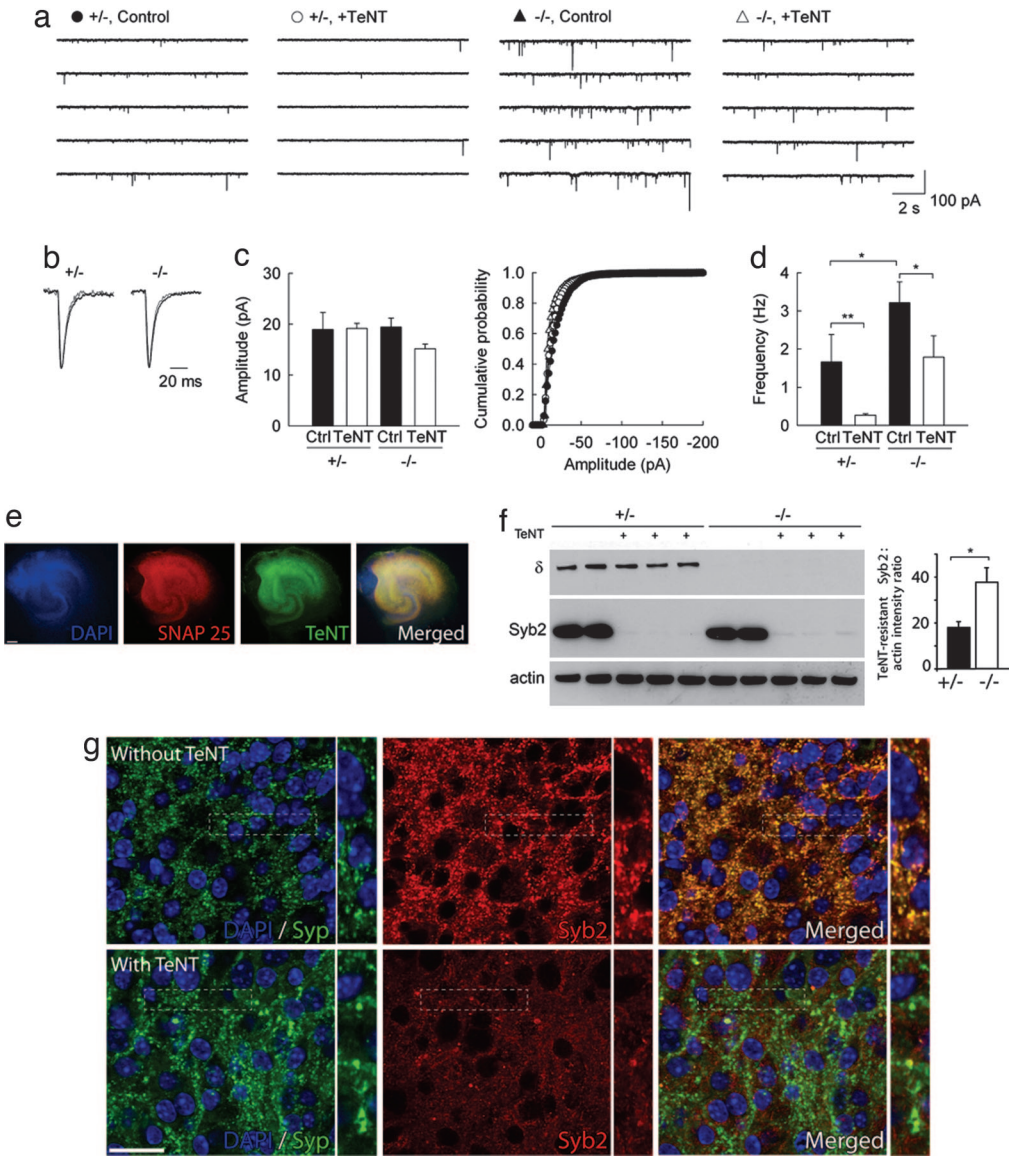

Fig. 3. Ca-independent quantal release at excitatory synapses on CA3 cells in control and *mocha* cultured slices. (*a*) Representative traces of mEPSCs recorded in CA3 pyramidal cells from control (+/−) and *mocha* (−/−) cultures, treated or not with TeNT. (*b*) Averaged mEPSCs (≈100) detected from the above recordings. Black traces, control; blue traces, after TeNT treatment. No difference in their rate of either onset or decay was apparent. (*c*) (*Left*) Average amplitude of mEPSCs recorded in all four conditions. No significant difference was observed ($n = 7$, 9, 11, and 8 cells, respectively; $P > 0.05$). (*Right*) Cumulative amplitude histograms from the same four data sets. The distributions were not significantly different (Kolmogorov–Smirnov test, $P > 0.05$). (*d*) Mean frequencies of mEPSCs were significantly different between control and TeNT-treated cultures in both control and mocha cultures ($P < 0.005$ and $P < 0.05$, respectively). mEPSC frequency was also different in control vs. mocha culture in the absence of TeNT ($P < 0.05$). (*e*) *mocha* culture slices treated with TeNT for 72 h were fixed and labeled with antibodies against SNAP25 (red), TeNT (green), and DAPI (blue). The whole surface of the explant can be visualized by either DAPI (nucleus) or SNAP25 (neuronal plasma membrane). Note that TeNT staining is uniformly distributed, confirming the extended penetration of the toxin. (Scale bar, 200 μm.) (*f*) Culture slices used in electrophysiological recordings were lysed and analyzed by Western blotting with antibodies against AP-3δ, Syb2, and actin (as a loading control). A 72-h treatment with TeNT resulted in efficient cleavage of Syb2, although quantification of the remaining Syb2 revealed a 2-fold increase in TeNT-resistant Syb2 in *mocha* slices [mean ± SEM; control 17.83 ± 2.35, $n = 6$; *mocha* 37.58 ± 6.31, $n = 6$; $P < 0.015$ (Mann–Whitney rank sum test)]. (*g*) *mocha*-cultured slices treated with or without TeNT for 72 h were fixed and labeled with antibodies against Syp (green), Syb2 (red), and DAPI (blue). Note that the remaining Syb2 labeling after TeNT treatment is very faint. The rare remaining Syb2 puncta are mainly synaptic. (Scale bar, 50 μm.)

www.pnas.org/cgi/doi/10.1073/pnas.0611561104